Eighth-order phase-field-crystal model for two-dimensional crystallization

A. Jaatinen[1,2] and T. Ala-Nissila[1,3]
[1]*Department of Applied Physics, Aalto University School of Science, P.O. Box 11000, FI-00076 Aalto, Finland*
[2]*Department of Materials Science and Engineering, Aalto University School of Science, P.O. Box 16200, FI-00076 Aalto, Finland*
[3]*Department of Physics, Brown University, Providence, Rhode Island 02912-1843, USA*
(Received 22 June 2010; revised manuscript received 19 November 2010; published 13 December 2010)

We present a derivation of the recently proposed eighth-order phase-field crystal model [A. Jaatinen *et al.*, Phys. Rev. E **80**, 031602 (2009)] for the crystallization of a solid from an undercooled melt. The model is used to study the planar growth of a two-dimensional hexagonal crystal, and the results are compared against similar results from dynamical density functional theory of Marconi and Tarazona, as well as other phase-field crystal models. We find that among the phase-field crystal models studied, the eighth-order fitting scheme gives results in good agreement with the density functional theory for both static and dynamic properties, suggesting it is an accurate and computationally efficient approximation to the density functional theory.

DOI: 10.1103/PhysRevE.82.061602 PACS number(s): 81.10.−h, 61.50.Ah, 61.72.Bb, 61.72.Mm

I. INTRODUCTION

Understanding crystal formation from an undercooled melt is of significant academic interest due to the complex phenomena involved in crystallization, and also of practical interest due to its relevance to a vast amount of industrial processes. During the past decade, rapidly evolving progress in microscopic understanding of phenomena involved in solidification has followed the introduction of the phase-field crystal (PFC) model [1,2]. This model was first introduced as a phenomenological extension of the traditional phase-field models [3] such that the order parameter field exhibits the crystalline nature of the underlying crystal lattice. The most significant advantage of PFC type of models over the traditional phase-field models is that including the periodic structure of the field in the model will naturally result in inclusion of many crystal structure related properties, such as elasticity, plasticity, and grain boundaries [1]. Since its introduction, the PFC model has been applied to modeling elastic and plastic deformation of materials [2,4], dislocation dynamics [5], crystal growth [6,7], static and dynamic properties of driven two-dimensional overlayers [8–10], etc.

Because of the periodic nature of the order parameter field in the PFC model, it is not hard to come up with an intuitive interpretation that the field must be related to the atomic number density of the underlying system. On the other hand, studies of classical density functional theory (DFT), most commonly in the context of inhomogenous liquids [11], have aimed at a microscopic derivation of the static (and more recently dynamic [12]) properties of the systems under study by using the microscopic density as a field variable in the theory. The extension of this approach to crystallization is known as the DFT of freezing, which has, in its many forms, been applied to study freezing of many different classical systems with a varying degree of success [13,14]. In 2007, Elder *et al.* [15] introduced the idea that assuming the field under study in the PFC model to be linearly proportional to the atomic number density in the DFT, the PFC model can be viewed as a simplified version of the DFT, and showed that the free energy functional used in PFC studies can be derived from the DFT by making certain approximations. Wu and Karma [16] introduced another way of obtaining the parameters for the PFC model using a DFT-like approach. In a recent paper, the strengths and weaknesses of the approaches proposed in Refs. [15,16] were studied, and a new variant of the PFC model known as the eighth-order fitting model (EOF), which reproduces certain thermodynamic properties of the material under study significantly more accurately than the previously proposed methods, was proposed [17]. More recently, the EOF model has been applied to study grain boundaries [18] and homogenous nucleation [19] of body-centered cubic iron.

In the present work, we will present an alternative interpretation of the EOF model, in which the field under study in the EOF is related to the physical atomic number density through a convolution, which filters out the subatomic wavelength Fourier modes from the atomic number density. Using this interpretation, we are able to derive the free energy of the EOF model in a way which we believe is more consistent with the original DFT than the previously presented derivations. Predictions of the EOF model are then tested against the DFT and other related PFC models. While most studies of the PFC model's connection to DFT have concentrated on the free energy, i.e., the static properties of the model, we will also compare the predictions for crystal growth rates, which is a dynamical phenomenon. Similar comparison between crystal growth rates in DFT and PFC models has previously been published by van Teeffelen *et al.* who found the growth rates of colloidal crystals in the early stages of solidification agree relatively well between the DFT and their choice of PFC models (not including the EOF) [7]. In the present work, we aim at a more thorough assessment of the crystal front propagation in the DDFT and PFC models. Instead of the initial growth rate, we aim at assessing the steady-state front propagation velocity in both the diffusion controlled and interface kinetics controlled regimes using both DDFT and EOF models. In addition, the results from these models are compared to results of a more traditional fourth-order PFC approach, and the "PFC1" model that van Teeffelen *et al.* proposed, and argued to be a more accurate approximation to DFT than the other model utilized in their comparison [7]. We find that among the PFC models studied,

the EOF gives results in best agreement with the DFT for both static properties and crystal growth.

II. THEORY

We study solidification dynamics in a two-dimensional ensemble of Brownian particles interacting via an inverse twelfth-power pair potential,

$$v(r) = \epsilon\left(\frac{\sigma}{r}\right)^{12}, \tag{1}$$

where r is the interparticle separation, ϵ sets the energy scale and σ is the diameter of the particles. Due to scaling properties, all structural and thermodynamic properties of this model system only depend on the scaled density

$$\tilde{\rho} = \left(\frac{\epsilon}{k_B T}\right)^{1/6} \rho\sigma^2, \tag{2}$$

where $k_B T$ is the thermal energy scale and $\rho = N/A$ is the number of particles per unit area. According to molecular dynamics simulations of Broughton *et al.*, the equilibrium state of the system is a fluid at densities up to $\tilde{\rho}_l = 0.987$, and a hexagonal solid at densities above $\tilde{\rho}_s = 1.006$, while between these two densities the equilibrium state is a coexistence of the solid and liquid phases [20,21]. As we assume that hydrodynamic interactions and the inertial terms can be neglected, the equations of motion for the particles are given by

$$\dot{\mathbf{r}}_i = \gamma^{-1}(\mathbf{F}_i + \mathbf{f}_i), \quad i = 1 \ldots N, \tag{3}$$

where the dot denotes time derivative, γ is a friction coefficient, $\mathbf{F}_i$ is the force from the other particles and an external field acting on particle i, and $\mathbf{f}_i$ is a Gaussian random force that fulfills the fluctuation-dissipation theorem.

A. Dynamical density functional theory

In the DDFT approach, instead of solving the positions of individual particles as a function of t, one derives an equation of motion for the one-particle density defined by

$$\rho(\mathbf{r},t) = \sum_i \langle \delta[\mathbf{r} - \mathbf{r}_i(t)] \rangle, \tag{4}$$

where the angular brackets denote a noise average [7]. Marconi and Tarazona [12] have shown that from the equations of motion (3), one can derive an equation of motion for $\rho(\mathbf{r},t)$ through a coordinate transformation and a subsequent noise averaging. In another procedure, Archer and Evans [22] have derived the same equation of motion by using the Smoluchowski equation as their starting point. The equation of motion for $\rho(\mathbf{r},t)$ resulting from both of these derivations reads

$$\dot{\rho}(\mathbf{r},t) = \gamma^{-1} \nabla \left[\rho(\mathbf{r},t) \nabla \left(\frac{\delta F[\rho(\mathbf{r},t)]}{\delta \rho(\mathbf{r},t)} \right) \right], \tag{5}$$

where $F[\rho(\mathbf{r},t)]$ is the Helmholtz free energy of the system described by a density field $\rho(\mathbf{r},t)$. As noted in the recent work of Ramos *et al.* this equation of motion can also be obtained in the overdamped limit of a more general equation of motion for the number and momentum densities, if the effective Hamiltonian is replaced by the free energy and thermal fluctuations are ignored [23].

The free energy F consists of three parts, $F = F_{id} + F_{ex} + F_{xs}$, where the first term represents the ideal gas contribution,

$$F_{id} = k_B T \int d\mathbf{r} \rho(\mathbf{r}) \{ \ln[\rho(\mathbf{r}) \lambda_T^2] - 1 \}, \tag{6}$$

where λ_T is thermal de Broglie wavelength and the second term is a contribution from an external field,

$$F_{ex} = \int d\mathbf{r} \rho(\mathbf{r}) u_{ex}(\mathbf{r}), \tag{7}$$

where $u_{ex}(\mathbf{r})$ is an external field acting on the particles. The third part of F is the excess, which is due to the interparticle interactions. For this quantity, exact expressions only exist for a very limited range of cases, and more generally, approximations will have to be made [11]. In the present work, we will use the simplest possible nonlocal approximation that is an expansion of F_{xs} in powers of $\Delta\rho = \rho - \rho_0$ around a uniform reference density ρ_0, where

$$F_{xs} = -k_B T \int d\mathbf{r} c^{(1)}(\rho_0) \Delta\rho(\mathbf{r}) - \frac{k_B T}{2} \times \int \int d\mathbf{r} d\mathbf{r}' \Delta\rho(\mathbf{r}) c^{(2)}(|\mathbf{r} - \mathbf{r}'|, \rho_0) \Delta\rho(\mathbf{r}'), \tag{8}$$

where $c^{(n)}$ are called nth order direct correlation functions. The quantity $c^{(2)}$ is the Ornstein-Zernike direct correlation function that can be obtained from experiments, computer simulations or a number of approximate closure relations to the Ornstein-Zernike equation [11]. In the present work, we will utilize the well-known Percus-Yevick closure relation with the pair potential Eq. (1) to obtain $c^{(2)}$. The reference density ρ_0 is chosen such that F has two equal minima: the trivial uniform minimum $\rho(\mathbf{r}) = \rho_0$ and another where $\rho(\mathbf{r})$ has a hexagonal structure (the external field u_{ex} is set to zero). This is the procedure taken in most DFT studies of freezing, and the resulting ρ_0 is interpreted as the freezing point of the liquid. Indeed, the free energy functional defined by Eqs. (6) and (8) is the simplest free energy functional used in static DFT studies of freezing, and its success has varied from case to case ([14] and references therein). The free energy defined by Eqs. (6) and (8) is also the free energy functional to which Elder *et al.* attempted to connect the free energy used in PFC studies [15].

Putting our free energy functional (with $u_{ex} = 0$) together with Eq. (5), and rescaling the density field variable as $\rho(\mathbf{r},t) = \rho_0[1 + n(\mathbf{r},t)]$, we end up with an equation of motion

$$\frac{\partial n}{\partial \tau} = \nabla^2 n - \nabla \left[(1+n) \nabla \int d\mathbf{r}' C(|\mathbf{r} - \mathbf{r}'|) n(\mathbf{r}') \right], \tag{9}$$

where the rescaled time $\tau = \gamma^{-1} k_B T t$ and $C = \rho_0 c^{(2)}$. Very few studies of the dynamics of crystallization using Eq. (9) are found in the literature. Van Teeffelen *et al.* have studied the dynamics of colloidal crystal nucleation and found results

that seemed to agree well with the results of molecular dynamics simulations [24]. The same group has studied the initial growth velocity of a colloidal crystallization front using Eq. (9) and compared the results against the results obtained from the PFC model [7]. To our knowledge, no other attempts to assess solidification dynamics by direct application of Eq. (9) exist in the literature.

B. Eighth-order phase-field crystal model

The eighth-order phase-field crystal model (EOF) was recently presented in Ref. [17] in the context of quantitative modeling of body-centered cubic iron. In that case, the model was shown to reproduce the anisotropic solid-liquid interfacial free energies, bulk moduli of solid and liquid phases, and the equilibrium coexistence gap between them to a quantitatively satisfactory precision. While some of these properties had been reproduced in previous versions of phase-field crystal models, the combination seemed inaccessible without the eighth-order extension [17]. In a subsequent study, it was shown that the EOF is also capable of describing grain boundary energies of bcc iron quantitatively [18].

Despite its quantitative success, there remain open issues in the EOF model. First, the previously presented derivation of the EOF is based on the assumption that the field n, related to the atomic number density as in the case of DFT, is small, such that the logarithmic term in the free energy could be expanded as a power series. However, it is well known that the actual atomic number density in the solid resembles a set of highly localized Gaussians, which does not agree with the assumption of n being small. Neither does it suggest that the nonlocal part of the free energy could be assumed local in k-space, as must be assumed, when expanding the direct correlation function in k-space around its main maximum. The equilibrium n-field resulting from these approximations is highly localized in k-space, having little resemblance to the Gaussian-like density obtained from the DFT. Most prominently, in the supposedly empty spaces between the lattice sites, the field n resulting from the EOF reaches values smaller than -1, corresponding to unphysical negative densities.

In what follows, we will present an alternative derivation of the EOF model which, although far from exact, avoids the previously mentioned caveats. The key to our derivation is the obvious fix in the interpretation of the field n used as the field variable in the EOF model: instead of insisting that the field n in the EOF model would be locally and linearly related to ρ in the same way as in the DDFT model, we will assume they are related through a weighing function w as

$$n(\mathbf{r}) = \rho_0^{-1} \int d\mathbf{r}' w(|\mathbf{r} - \mathbf{r}'|)[\rho(\mathbf{r}) - \rho_0]. \tag{10}$$

In the current approach, the weighing procedure introduced in Eq. (10) will act as a Fourier filter, cutting off the short wavelength modes of ρ that have very small amplitude in the periodic solutions of the PFC model. In other words, the field n in the bulk of the solid phase will closely resemble the one-mode approximation,

$$n(\mathbf{r}) \approx n_0 + 2u\left[\cos\left(\frac{4\pi y}{\sqrt{3}d_{nn}}\right) - 2\cos\left(\frac{2\pi x}{d_{nn}}\right)\cos\left(\frac{2\pi y}{\sqrt{3}d_{nn}}\right)\right], \tag{11}$$

where n_0 is the fractional density change and d_{nn} is the nearest-neighbor distance, even though the underlying density field were highly peaked around lattice sites.

A convenient choice for w is a function, whose Fourier transform is given by

$$\hat{w}(k) = \sqrt{\frac{1 - \hat{C}(k)}{1 - \hat{C}_{EOF}(k)}}, \tag{12}$$

where $C_{EOF}(k)$ is the "approximation" to $C(k)$ introduced in [17],

$$\hat{C}_{EOF}(k) = \hat{C}(k_m) - E_S\left(\frac{k_m^2 - k^2}{k_m^2}\right)^2 - E_B\left(\frac{k_m^2 - k^2}{k_m^2}\right)^4, \tag{13}$$

where k_m is the position of the main peak in $\hat{C}(k)$, E_S is chosen such that second derivatives at the peak of the original and the approximated curves are equal, and E_B is then chosen such that the infinite-wavelength ($k=0$) limits are equal. The function $\hat{C}_{EOF}(k)$ will follow the original $\hat{C}(k)$ very closely from the $k=0$ limit up to the main peak at k_m, after which the two curves diverge, $\hat{C}(k)$ approaching zero in an oscillatory fashion, while $\hat{C}_{EOF}(k)$ falls in the negative infinity, such that $\hat{w}(k)$ defined by Eq. (12) will fall close to zero rapidly after the main peak, providing the desired Fourier filter property mentioned earlier.

What makes the choice of $\hat{w}(k)$ defined by Eq. (13) particularly convenient is that the linear part of the free energy [linearization of Eqs. (6) and (8)] can now be exactly written as

$$\frac{\beta F_{lin}}{\rho_0} = \frac{\rho_0^{-2}}{2}\int\int d\mathbf{r}d\mathbf{r}'\Delta\rho(\mathbf{r})[\delta(\mathbf{r} - \mathbf{r}') - C(\mathbf{r} - \mathbf{r}')]\Delta\rho(\mathbf{r}')$$
$$= \frac{1}{2}\int d\mathbf{r} n(\mathbf{r})[1 - C_{EOF}(\nabla^2)]n(\mathbf{r}), \tag{14}$$

where δ is the Dirac delta function and $C_{EOF}(\nabla^2)$ is the inverse Fourier transform of $\hat{C}_{EOF}(k)$, i.e., Eq. (13) with $-k^2$ replaced by ∇^2.

Unfortunately for the nonlinear parts of the free energy,

$$\beta F_{nl} = \beta(F - F_{lin}) = \int d\mathbf{r}\left\{\rho(\mathbf{r})\ln[\rho(\mathbf{r})/\rho_0] - \Delta\rho(\mathbf{r}) - \frac{\Delta\rho(\mathbf{r})^2}{2\rho_0}\right\}, \tag{15}$$

the situation is not nearly as trivial because the expressions will become both nonlocal and nonlinear. However, as we know that F_{lin} defined by Eq. (14) already provides us with both a preferred wavelength of fluctuations in the system, and a large free energy penalty for Fourier modes with $k \gg k_m$, we argue that if the amplitudes u in Eq. (11) vary on length scales larger than the range of the weighing function, it may be sufficient to approximate F_{nl} with a functional that

is local in terms of the field n. To fit this purpose, we postulate a simple, local, nonlinear functional, consisting of third and fourth-order terms,

$$\frac{\beta F_{nl,EOF}}{\rho_0} = \int d\mathbf{r}\left(-\frac{a}{6}n(\mathbf{r})^3 + \frac{b}{12}n(\mathbf{r})^4\right), \tag{16}$$

where a and b are phenomenological constants. As a consequence of this crude approximation, ignoring practically all information about the Fourier modes with $k \gg k_m$, it is admittedly obvious that the density field obtained from a solution of the EOF model through inverting Eq. (10) will not be an accurate approximation to the real underlying density field, unless a more accurate approximation to F_{nl} will be presented in subsequent studies.

It should be noted that the free energy functional for the EOF obtained by summing up Eqs. (14) and (16) is exactly the same as used in previous EOF studies [17,18]. One crucial difference, in addition to the different approximations involved, is that the current derivation does not suggest that $a=b=1$, like the previous version, based on Taylor expansion, did [17]. Instead, in the current approach, it is clear that the proper way to choose parameters a and b is such that free energies of relevant density profiles are reproduced as accurately as possible (in the end, to correct for the flaws in the derivation, fitting the parameters a and b with the desired amplitude of the solid phase was the approach taken in the previous studies as well). In order to gain insight into how these parameters should be chosen, consider a density field consisting of an infinite set of normalized Gaussians in a triangular lattice,

$$\rho(\mathbf{r}) = \sum_i \frac{\alpha}{\pi} e^{-\alpha|\mathbf{r}-\mathbf{R}_i|^2}, \tag{17}$$

where $\mathbf{R}_i$'s are positions of lattice points that belong in the underlying hexagonal lattice. It is well known that in the bulk of the solid, this is a fairly accurate approximation to the density profile that results from DFT of freezing [14]. More specifically, consider the case when the density of lattice points $2/(\sqrt{3}d_{nn}^2)=\rho_0$ and the length of the principal reciprocal lattice vector $|\mathbf{G}_m|=4\pi/(\sqrt{3}d_{nn})$ coincides with position of the main peak in $\hat{C}$, i.e., $|\mathbf{G}_m|=k_m$. Then, through Eqs. (10) and (12), the field n will be closely approximated by Eq. (11), with $n_0=0$, and the amplitude u is related to the Gaussian parameter α as

$$u = e^{-|\mathbf{G}_m|^2/2\alpha}. \tag{18}$$

It is then straightforward to calculate from Eqs. (14) and (16) that free energy of the system described by this single-mode n field will be given by

$$\frac{\beta F_{EOF}}{N} = 3[1-\hat{C}(k_m)]u^2 - 2au^3 + \frac{15}{2}bu^4. \tag{19}$$

In what follows, this expression will be related to the small and large α limits of the original free energy, given by Eqs. (6) and (8), in the Gaussian approximation.

In the limit of small α, deviations from uniformity in the density field are small, and therefore, instead of the full free energy functional, it is sufficient to consider the linearized version defined by Eq. (14),

$$\frac{\beta F}{\rho_0} \approx \frac{\rho_0^{-2}}{2}\int\int d\mathbf{r}d\mathbf{r}'\Delta\rho(\mathbf{r})[\delta(\mathbf{r}-\mathbf{r}') - C(\mathbf{r}-\mathbf{r}')]\Delta\rho(\mathbf{r}')$$
$$= \frac{1}{2}\sum_i [1-\hat{C}(|\mathbf{G}_i|)]e^{-|\mathbf{G}_i|^2/\alpha} \tag{20}$$

where the sum is over all nonzero reciprocal lattice vectors. Using Eq. (18), this can be rewritten in terms of u as

$$\frac{\beta F}{\rho_0} \approx \frac{1}{2}\sum_i [1-\hat{C}(|\mathbf{G}_i|)]u^{2(|\mathbf{G}_i|/|\mathbf{G}_m|)^2}. \tag{21}$$

Now it is easily observed that in the limit where u is small, the leading contribution to the sum in Eq. (21) comes from the shortest reciprocal lattice vectors, for which $|\mathbf{G}_i|=|\mathbf{G}_m|$. As the number of vectors in this first star of reciprocal lattice vectors is six, we obtain exactly the same small-u behavior from Eqs. (19) and (21). This result may not be surprising, due to the exact relation between the linear parts of free energies in the models.

In the limit of large α, i.e., highly localized density peaks, the free energy can be accurately evaluated by ignoring the overlap between peaks in the ideal gas term [14], resulting in

$$\frac{\beta F}{N} \approx \ln\left(\frac{\alpha}{\pi\rho_0}\right) - 1 - \frac{1}{2}\sum_i \hat{C}(|\mathbf{G}_i|)e^{-|\mathbf{G}_i|^2/\alpha}. \tag{22}$$

Using Eq. (18), this can also be expressed as a function of u as

$$\frac{\beta F}{N} \approx \ln\left(\frac{2\pi}{\sqrt{3}e}\right) - \ln[-\ln(u)] - \frac{1}{2}\sum_i \hat{C}(|\mathbf{G}_i|)u^{2(|\mathbf{G}_i|/|\mathbf{G}_m|)^2}. \tag{23}$$

We note that it might be possible to come up with a form of $F_{nl,EOF}$ that would resemble this form more closely than the simple fourth-order polynomial in Eq. (19). For the time being, however, we find it sufficient to study the implications of Eq. (23) to the parameters a and b of Eq. (16). Perhaps the most interesting of these implications is the contribution of the ideal gas term in the parameters a and b. Ignoring all terms that are proportional to $\hat{C}(k)$ in Eqs. (19) and (23) leaves us with the problem of finding coefficients a_{id} and b_{id} (subscript id refers to the ideal free energy), such that

$$3u^2 - 2a_{id}u^3 + \frac{15}{2}b_{id}u^4 \approx \ln\left(\frac{2\pi}{\sqrt{3}e}\right) - \ln[-\ln(u)]. \tag{24}$$

There are, of course, an infinite number of ways to perform this fit. After experimenting with least-squares fits on different intervals of u, we found that for example by choosing $a_{id}=3/4$ and $b_{id}=1/5$, we obtain a reasonably good agreement between the two curves over a large interval of u, as shown in Fig. 1. Even though details in the fitting procedure will affect the obtained numbers to some extent, a common feature observed in all reasonable fits is that the parameter a_{id} is always on the order of 1, while b_{id} is almost an order of magnitude smaller. Thus, this argument explains why the pa-

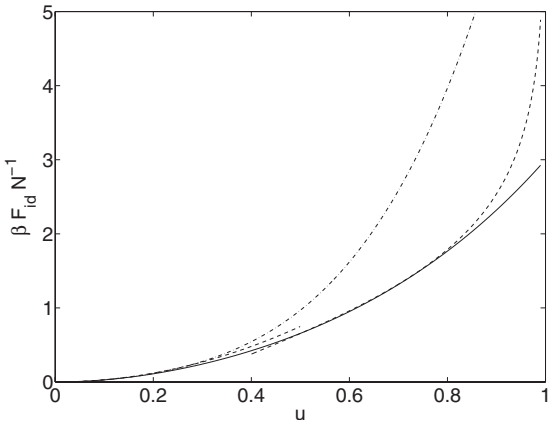

FIG. 1. Ideal free energy as a function of u in the one-mode approximation to the EOF model, as indicated in Eq. (24) with $a_{id}=3/4$ and $b_{id}=1/5$ (solid line). Dashed lines represent the small- and large-u limits obtained from the original F_{id} in the Gaussian approximation. For comparison, the dashed-dotted line shows the curve expected from a Taylor expansion of F_{id} (i.e., $a_{id}=b_{id}=1$) which is seen to significantly overestimate F_{id}.

rameters that were observed to be practicable in our previous studies [17] were so different from unity, suggested by the naive Taylor expansion of the log-term.

Further refinement to the parameters a and b could be obtained by studying the terms related to $\hat{C}(k)$ in Eq. (23). However, as the expressions for ρ and n used in deriving Eqs. (19) and (23), we suggest using numerical fitting methods in order to achieve maximum accuracy. In order to find a functional, that gives such a field n that best approximates the original DFT, the most obvious choice is to find such a and b that a numerical free energy minimization results in the same u as obtained from the DFT, and the solid that exhibits this u coexists with the liquid phase (given that is the case in the original DFT functional as well).

For dynamics of the EOF model, we use the form widely used in PFC studies, i.e.,

$$\frac{\partial n}{\partial \tau} = \nabla^2\left(\frac{\delta F_{EOF}}{\delta n}\right) = \nabla^2\left\{[1-\hat{C}(k_m)]n - \frac{a}{2}n^2 + \frac{b}{3}n^3 + E_S\left(\frac{k_m^2+\nabla^2}{k_m^2}\right)^2 n + E_B\left(\frac{k_m^2+\nabla^2}{k_m^2}\right)^4 n\right\}, \tag{25}$$

where τ is defined as earlier. Motivation to choosing this equation of motion is that it is probably the minimum complexity model satisfying the usual requirements for conserving the total mass and evolving toward minimum of the free energy, that also catches approximately the same dynamics as the DDFT in the near-uniformity limit, for the relevant Fourier modes up to k_m [linearized version of Eq. (9) is $\partial_\tau \hat{n}(k) = -k^2[1-\hat{C}(k)]\hat{n}(k)$, while that of Eq. (25) would be the same, but with $\hat{C}$ replaced by $\hat{C}_{EOF}$]. For studying solidification, we believe the limit of near-uniformity is the dominant factor affecting the solidification front velocity, even though some details of the dynamics on the solid side of the front may have a secondary effect on the front propagation.

C. Other phase-field crystal models

In addition to comparing the results of the EOF model with those of the DDFT model, we will also compare their results to two other PFC models presented in the literature. The first model we will include is essentially the Swift-Hohenberg (SH) model used in almost all the PFC studies up to date. Where the EOF model contains gradients up to eighth order in the linear part of the free energy, the SH formulation only contains gradients up to fourth order. The procedure we use for obtaining parameters for the SH model such that it could be used to model real parameters is essentially the one introduced by Wu and Karma [16]. In the framework of the present work, we may also view the SH-based approach an approximation to the EOF, where $E_B=0$, and the parameters a and b are fitted through the same procedure as in the EOF. The equation of motion for this model, which we will call the fourth-order fit (FOF) for the remainder of this paper, becomes

$$\frac{\partial n}{\partial \tau} = \nabla^2\left\{[1-\hat{C}(k_m)]n - \frac{a}{2}n^2 + \frac{b}{3}n^3 + E_S\left(\frac{k_m^2+\nabla^2}{k_m^2}\right)^2 n\right\}, \tag{26}$$

We note here that even though many formulations of the SH-based PFC models do not include the third order term $-an^3/6$ in the free energy, it has been shown that the model without that term can be exactly recovered from Eq. (26) after appropriate scaling of the field variable and the parameters [25].

In addition to the FOF and EOF models, another interesting PFC model was proposed in the recent work of van Teeffelen *et al.* [7]. In the model they call PFC1, they start with the DDFT, and approximate the function $\hat{C}(k)$ by expanding it around k_m in a fourth-order power series, in a similar manner as in the FOF model. However, as the excess part of the free energy in this approach would not be sufficient to stabilize the solid at any reasonable density [7,17], the excess part of the free energy is multiplied by a scaling factor α. Thus, the equation of motion in this model becomes

$$\frac{\partial n}{\partial \tau} = \nabla^2 n - \alpha\nabla\left((1+n)\nabla\left\{\left[\hat{C}(k_m) - E_S\left(\frac{k_m^2+\nabla^2}{k_m^2}\right)^2\right]n\right\}\right). \tag{27}$$

Using arguments based on a single mode approximation to the free energy of the solid, van Teeffelen *et al.* come up with $\alpha=1.15$ for the case of colloids interacting via r^{-3} potential which they studied [7]. In the present work, we will utilize numerical fitting methods to find an α, such that the correct freezing point from the DFT is reproduced in the PFC1 model. Van Teeffelen *et al.* also showed that this PFC1 model performs slightly better than their "PFC2" model, which is based on FOF with $a=b=1$ and $\alpha=1.15$, in reproducing the initial crystallization velocities of the DDFT, ar-

guing that the better success is due to fewer approximations made in the derivation [7]. In the following, we shall see how the PFC1 model compares with EOF and FOF for the case under study in the present paper.

III. STATIC RESULTS AND MODEL PARAMETERS

In order to find the freezing density of the fluid in the DFT model, we have calculated the direct correlation function for the pair potential defined by Eq. (1) at different densities by using the well-known Ornstein-Zernike equation together with the closure relation by Percus and Yevick (PY) [26]. At each density, we then find the nontrivial minimum of the free energy, in which the density field has a hexagonal structure (at densities where it exists), by a similar free energy minimization method as utilized in [17]. Of the minimization method, it is worthy of noting that unlike in most DFT studies [7,14] (and like in [17]), we do not restrict the calculations to a perfect lattice (i.e., zero vacancy concentration) constraint, for the reason that in a dynamical simulation, it is not possible to control this issue without modifying the free energy.

Repeating the procedure of finding the direct correlation function and the solid minimum of free energy at many different reference densities, we find that freezing occurs at $\tilde{\rho}_l = 0.9156$, because for that reference density, the minimum free energy of the solid equals that of the liquid at $\rho = \rho_0$. That is also the reference density ρ_0 that will be used for all the calculations in the remainder of this paper. Compared with the previously mentioned result from molecular dynamics simulations, this result is an underestimation of the freezing density by approximately 7%. This difference could be due to multiple sources of error, including approximating F_{xs} by Eq. (8), the PY closure relation or not including the perfect lattice constraint. However, for our purposes, the result is acceptable, especially given that the width of the coexistence gap $\Delta\rho^* = (\rho_s - \rho_l)/\rho_l \approx 2\%$ [21] is reproduced well: our DFT result is $\Delta\rho^* = 2.20\%$.

From the direct correlation function at freezing point, we find the PFC model parameters $k_m = 6.3965/\sigma$, $\hat{C}(k_m) = 0.7855$, $E_S = 14.5487$, and $E_B = 63.7814$. The direct correlation function, together with the expansions of EOF [Eq. (13)] and FOF [Eq. (13) with $E_B = 0$] are shown in Fig. 2. As mentioned in the previous section, for the EOF and FOF models, the parameters a and b are then defined such that the solid phase coexists with the liquid phase at $\rho = \rho_0$, and the amplitude of Fourier modes corresponding to the first star of reciprocal lattice vectors of the solid phase

$$u_s = \int d\mathbf{r} n(\mathbf{r}) e^{i\mathbf{G}\cdot r}, \tag{28}$$

where $\mathbf{G}$ is any reciprocal lattice vector from the first star, equals that obtained from the DFT, $u_s = 0.7914$. Based on numerical iteration, these two constraints yield $a = 0.8082$ and $b = 0.1388$ for the EOF, which are notably rather close to the values of a_{id} and b_{id} presented in the previous section. For FOF, the same fitting procedure results in only slightly different numbers, $a = 0.7812$ and $b = 0.1438$. For PFC1, the parameter α is chosen to fulfill only first of the constraints for EOF and FOF, i.e., that the solid coexists with the liquid at $\rho = \rho_0$. This yields $\alpha = 1.1934$.

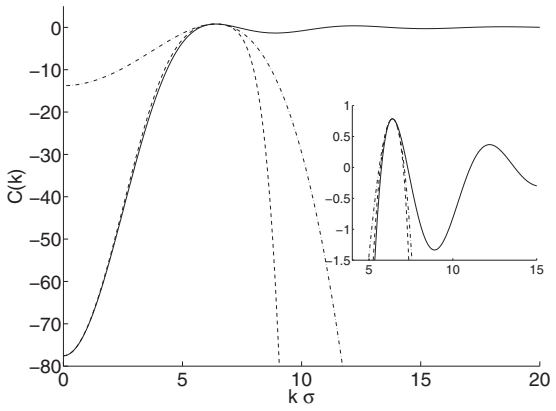

FIG. 2. Direct correlation function at $\tilde{\rho}_l = 0.9156$ as obtained from the PY closure relation (solid line), and the fitted EOF (dashed line) and FOF (dashed-dotted line) expansions.

As expected [7,17], the solid state density profiles we find from the DFT are much more peaked around the lattice sites. From all PFC models, we find the field n resembles the one-mode approximation rather closely. The n fields found from EOF and FOF are very similar to each other, and to the field obtained from the DFT through filtering the higher order Fourier modes in the density. The solution from PFC1 differs from the two other PFC models in that the amplitude of density fluctuations is $u_s = 0.2051$, which is smaller than in the DFT and the other PFC models by about a factor four. The coexistence gap $\Delta\rho^*$ is 1.57% in the EOF, 7.70% in the FOF, and 0.68% in the PFC1. Comparing the coexistence gaps of the PFC models with the previously mentioned results from molecular dynamics and DFT, the EOF gives the closest, although not perfect result. In FOF, too small a bulk modulus results in too large a coexistence gap [17]. In PFC1, the small u_s and $\Delta\rho^*$ indicate that the transition from solid to liquid is a weaker first order transition than in the two other models.

We have also studied properties of the solid-liquid interface in these models in the close-packed [10] direction. Due to scaling properties of the potential, the interfacial free energy of the system is given by

$$\Gamma = \frac{k_B T}{\sigma}\left(\frac{k_B T}{\epsilon}\right)^{1/6}\tilde{\Gamma}, \tag{29}$$

where $\tilde{\Gamma}$ is the dimensionless interfacial free energy in rescaled units. Initializing a system with a slab of solid at $\tilde{\rho}_s$ in the middle of a liquid at $\tilde{\rho}_l$, we find after numerical free energy minimization $\tilde{\Gamma} = 0.234$ in the DFT. From the EOF and FOF we find almost exactly the same interfacial energies, i.e., $\tilde{\Gamma} = 0.222$ in the EOF and $\tilde{\Gamma} = 0.223$ in the FOF. These results also agree rather well with the DFT result. On the other hand, from PFC1 we find $\tilde{\Gamma} = 0.0086$, which is more than an order of magnitude smaller than in all the other models. Density profiles of the interface layer in the different

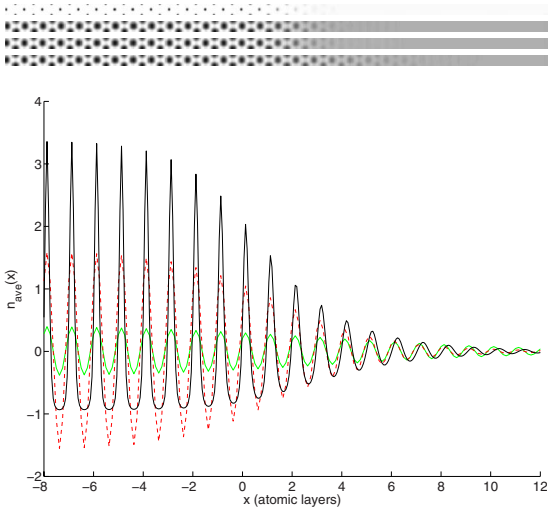

FIG. 3. (Color online) On the top, we show density profiles of the solid-liquid interface, from top to down, in the DFT, EOF, FOF, and PFC1 models. Darker shades of gray correspond to larger densities in these images, with a scale such that the maximum of n in each case corresponds to black, and minimum to white. In the lowest image, we show the field n averaged in the direction parallel to the interface, as a function of the spatial coordinate perpendicular to the interface. Black solid line corresponds to DFT, red dashed line is EOF, and solid, light green line is PFC1 (FOF is not shown because it would be practically indistinguishable from EOF in this plot).

models are shown in Fig. 3. It can be seen that in PFC1, the interface layer is considerably wider than in all the other models, while the interface widths in EOF and FOF are very similar to that in the DFT. We are not aware of any computer simulation predictions for the surface free energy of r^{-12} disks.

As an aside, we note that the justification for a and b being different from unity presented in the previous section is not the only one published. Berry *et al.* [27] have noted that a local n^3 term can also be justified by considering the $k=k'=0$ contribution from a third order term in the density expansion of F_{xs}. Technically, this is equivalent to assuming that the density field is slowly varying compared with the range of three body correlations. If such term is included in Eq. (8), and the logarithm is expanded in a Taylor series, it is straightforward to derive an explicit expression for a,

$$a = 1 + \rho_0^2 \hat{c}^{(3)}(0,0), \tag{30}$$

where $\hat{c}^{(3)}(0,0)$ is the $k=k'=0$ mode of the three body direct correlation function. Using the Ornstein-Zernike relation with Percus-Yevick closure, $\hat{c}^{(3)}(0,0)$ can be calculated by noting that it is related to the $k=0$ mode of the two body direct correlation function through the sum rule

$$\hat{c}^{(3)}(0,0) = \frac{\partial \hat{c}^{(2)}(0;\rho_0)}{\partial \rho_0}. \tag{31}$$

The prediction for a we obtain from this approach is $a \approx -410$, which is not only large in terms of absolute value, but also has the wrong sign with respect to stabilizing the solid phase. Similar consideration for the fourth-order term b, considering $k=k'=k''=0$ contribution from the four-body correlation term, yields $b \approx 1.35 \times 10^3$. Based on these considerations, we conclude that our values for a and b cannot be justified in terms of higher order correlations.

IV. DYNAMICAL SIMULATIONS

The solidification front dynamics in the DDFT and the different PFC models were studied by growing a hexagonal crystal from an undercooled liquid (i.e., a liquid with an initial density $\rho_i > \rho_l$) in the [10] direction. In the direction perpendicular to the solidification front propagation, the size of the array in our computations is exactly one interparticle spacing, and periodic boundary conditions are used. Due to the periodic boundaries, our simulations represent an infinitely wide crystal seed that propagates into the liquid. That the size of our simulation box is only one interparticle spacing in the [01] direction means that no instabilities that could roughen the surface are allowed. Initial condition for the DDFT, EOF and FOF simulations is such that eight monolayers of perfect solid are placed in the middle of the undercooled liquid, with a slight smoothing in the boundary of solid and liquid phases, while for PFC1, we had to use a crystal seed of 12 monolayers in order to initialize the growth process at even the smallest undercoolings studied. Once the simulation starts, the solid seed grows in both directions, and we measure its position as a function of time. Position of the surface is defined as the point where a line drawn through the local maxima of the density corresponding to the solid particles reaches one half of its maximum value. In the direction of growth, the length of our array was usually 512 interparticle spacings.

For numerically integrating the EOF and FOF models, we use the well-known semi-implicit operator splitting method [28] with Fast Fourier transforms. For spatial resolution, we use $\Delta x = \sqrt{3} d_{nn}/16$ and $\Delta y = d_{nn}/16$ (d_{nn} is the nearest-neighbor distance), time step is $\Delta\tau = 10^{-3}$, and the Laplace operator is discretized in k-space as $\nabla^2_{\mathbf{k}} = -k^2$. For the DDFT, we employ a similar procedure, by treating the $\nabla^2 n$ term in Eq. (9) implicitly and the term related to F_{xs} explicitly. The nonlocal term is evaluated in k-space and derivatives in x and y directions are discretized in k-space as $ik_{x,y}$. For DDFT, in order to resolve the sharp density peaks, the linear spatial resolution of the PFC is doubled, i.e., $\Delta x = \sqrt{3} d_{nn}/32$ and $\Delta y = d_{nn}/32$. The time step we use for DDFT is $\Delta\tau = 10^{-3}$ in the regime of low undercooling. In the regime of high undercooling we found that retaining the numerical accuracy required us to decrease the time step to $\Delta\tau = 10^{-4}$, which is smaller than we utilized in EOF and FOF models by an order of magnitude. This, together with the difference in spatial resolution, means that using our methods, simulations with the DDFT are approximately two orders of magnitude slower than with the EOF and FOF models. For PFC1, we modified the method used for DDFT such that the implicitly treated part is $\nabla^2[1 - \alpha C_{PFC1}(\nabla^2)]n$, leaving $\alpha \nabla n \nabla [C_{PFC1}(\nabla^2) n]$ treated explicitly. Even though for PFC1 this modification brought great advantage in numerical stability, handling the nonlinear part still involves explicit evaluation of sixth de-

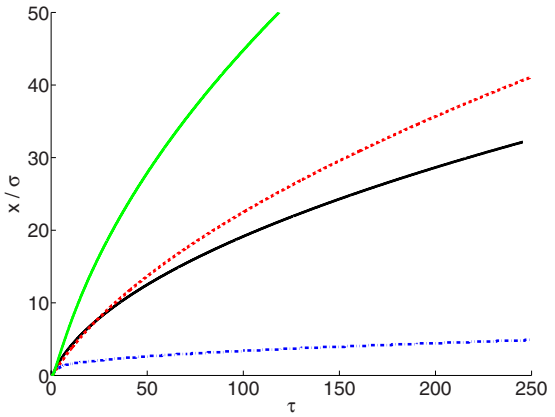

FIG. 4. (Color online) Interface position as a function of time when $\rho_i = 1.0044\rho_l$. Black solid line is the result obtained from the DDFT, red dashed line is from the EOF, blue dash-dotted line is from the FOF, and green solid line is from the PFC1.

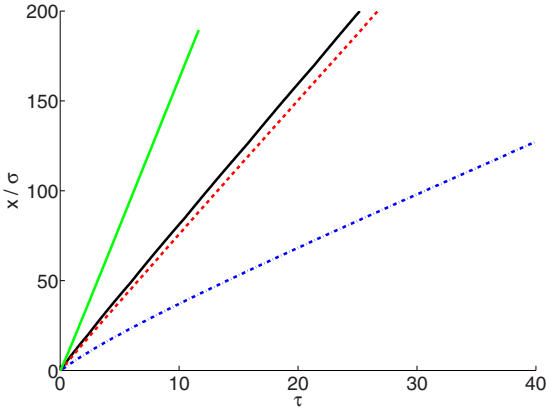

FIG. 5. (Color online) Interface position as a function of time when $\rho_i = 1.088\rho_l$. Different lines are as in Fig. 4.

rivative. Therefore, we found the PFC1 to be numerically most unstable among the models studied. In order to ease the requirement this model places on the time step, we dropped the spatial resolution perpendicular to growth below that used in other PFC models, to $\Delta y = d_{nn}/8$, which we did not find to have any profound effect on any results predicted by the model. However, this only allowed us to utilize time steps that are one order of magnitude smaller than in the DDFT, making the PFC1 numerically approximately equally demanding to DDFT using current methods. In addition to the differences in Δx, Δy, and $\Delta\tau$ between the models, we note that progressing a single time step in DDFT and PFC1 models requires a total of five Fourier (or inverse Fourier) transforms, where in EOF and FOF, only three are required.

If the undercooling is small, such that $\rho_i < \rho_s$, then formation velocity of the solid (whose density is always at least ρ_s to be stable) is expected to be limited by the diffusion of mass to the interface, in an analogous manner to the more commonly considered case where growth of the solid is limited by transport of heat away from the surface [29]. Density of the solid seed in these simulations is chosen to be that of the solid coexisting with the liquid. As the planar solidification front propagates, the layer through which diffusion must take place widens, and therefore one expects the solidification front to propagate as $x \sim \tau^{0.5}$. Diffusion-controlled growth in the PFC model has been previously studied by Tegze *et al.* [6], but to our knowledge, no studies of the subject utilizing a nonlocal DDFT have been published. On the other hand, when density of the liquid from which the solid is formed exceeds ρ_s, propagation of the solidification front does not require diffusion of additional mass to the surface. Therefore, one expects the front to propagate with a constant velocity, i.e., $x \sim t$, that depends on the attachment rate of particles on the interface.

The different regimes of growth, as well as differences between the different models, are illustrated in Figs. 4 and 5. In Fig. 5 we show the interface position as a function of time from all models, for a case where $\rho_i = 1.0044\rho_l$, which is in the $\Delta < 1$ regime of all models. At the very beginning of the solidification process, kinetics define how fast the particles attach to the interface from the liquid with a density ρ_i. During the initial stages, a depletion layer is formed in front of the liquid. As time goes on, width of the depletion layer increases, and $x(\tau)$ approaches the expected $x \sim \tau^{0.5}$ behavior. By close inspection of Fig. 4 it can be seen that at the very beginning of the process, interface motion in the PFC1 model is slightly faster than in the DDFT. On the other hand in the EOF and FOF models, the initial interface motion is slightly slower than in DDFT, indicating more restriction to growth due to interface kinetics. In the EOF and FOF models, the initial velocities are strikingly similar. On the other hand, Fig. 5 shows interface positions as a function of time for an initial density of $\rho_i = 1.088\rho_l$, which is in the $\Delta > 1$ regime of all models. Again, in the initial stages of solidification, a depletion layer is formed in front of the moving interface. However in this case the width of the depletion layer, and thus the propagation velocity of the interface, quickly approach constant values, and therefore the growth seems linear.

In order to quantify the detection of the different growth regimes, we have fitted a power law growth function,

$$x = x_0 + c(\tau - \tau_0)^{\alpha}, \tag{32}$$

in the surface positions as a function time resulting from the different models at different initial densities. The first quarter of the $x(\tau)$ data is ignored in these fits in order to minimize the effect from the initial stages, while still obtaining a fairly robust fit for the four free parameters. The exponents α resulting from these fits are shown in Fig. 6. The growth exponents obtained from the FOF and PFC1 models are in general close to the ideal results (even at unit undercooling, the observed exponent $\alpha \approx 0.70$ from FOF is close to the expected anomalous exponent $\alpha = 2/3$ [29,30]), whereas in DDFT and EOF models, the transition from the diffusion controlled to kinetics controlled regime seems more continuous. The discrepancy between observed and expected exponents is due to insufficient simulation time for the formation of the steady-state depletion layer in DDFT and EOF models. The discrepancy is most evident in the EOF model. This is most likely because the combination of small coexistence gap, fast diffusion in the solid, and relatively slow interfacial

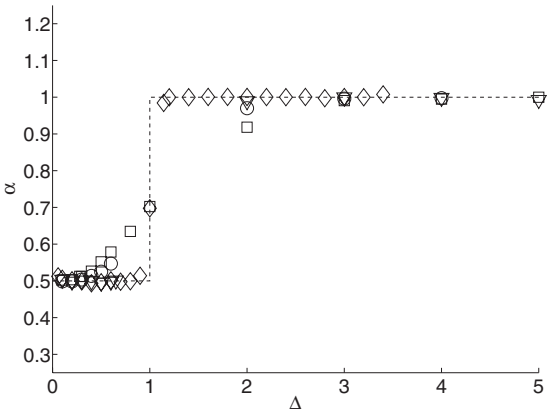

FIG. 6. Growth exponents obtained from the different models. Circles are results from DDFT model, squares from EOF, diamonds from FOF, and triangles from PFC1, while dashed line shows the ideal behavior.

kinetics makes the formation of a quasi-steady-state depletion layer in the EOF slowest among the models.

In the $\Delta < 1$ regime, we have quantified the effect of the initial density on the quasi-steady-state velocity of front propagation by fitting the $x(\tau)$'s resulting from different models for different ρ_i's with the expected growth law,

$$x = x_0 + d(\tau - \tau_0)^{1/2}, \tag{33}$$

ignoring the early stages where $x\sigma^{-1} < 50$. Equation (33) is mathematically equivalent to Eq. (32) with α set to 0.5. Despite the previously mentioned discrepancies between the observed and now preset growth exponents, we are able to obtain good fit with Eq. (33) for all models in the regime $\Delta \leq 0.6$, as shown in Fig. 7. The d resulting from these fits is shown in Fig. 8. Beyond $\Delta = 0.6$, we have less confidence in having reached close enough to a steady-state diffusion-controlled growth regime, especially in the EOF model, and therefore the data is only shown for undercoolings up to $\Delta = 0.6$.

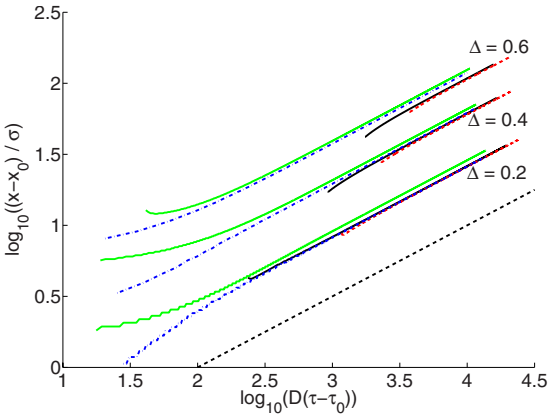

FIG. 7. (Color online) Logarithmic plot of rescaled interface positions as a function of rescaled time from different models in $\Delta \leq 0.6$ regime. The black dashed line shows the expected slope, while other lines are labeled as in Fig. 4.

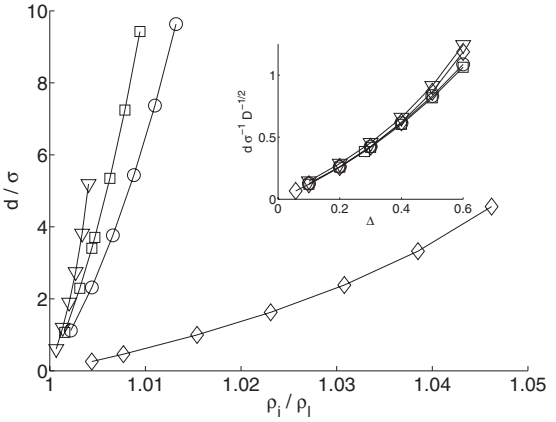

FIG. 8. Growth rates d obtained in the diffusion-controlled regime. Circles are results from DDFT model, squares from EOF, diamonds from FOF, and triangles from PFC1, with lines connecting the symbols. Inset shows scaled data.

It is seen in Fig. 8 that among the PFC models, the EOF in general gives the closest agreement with the DDFT. Due to scaling properties of the problem, if the growth were purely diffusion limited, one would expect the position of the interface to depend on the dimensionless undercooling Δ and $\sqrt{D\tau}$, where $D = 1 - \hat{C}(0)$ [for PFC1, multiply $\hat{C}(0)$ by α] is the effective diffusion constant in a given model (in the limit of small, long-wavelength density fluctuations, with this definition, all the models studied reduce to the diffusion equation $\partial_\tau n = D\nabla^2 n$). Such a scaling law for the growth rates is illustrated in the inset of Fig. 8, where we show that the d's scaled by $\sqrt{D}$ as a function of Δ in DDFT, EOF, and FOF models follow the same curve, indicating that differences in microscopic details of those models are unimportant in determining the front velocity in the diffusion-controlled regime. Results from PFC1 lie slightly above those from the other models in the rescaled plot, which we believe is most likely a result of numerical inaccuracy. These scaling properties of the problem are the reason why the EOF, which has exactly the same D and close to the same $\Delta\rho^*$ as DDFT, reproduces the result of the DDFT with higher accuracy than the FOF, which results in a d that is approximately an eighth of the result obtained from the DDFT for the same ρ_i. The scaling argument also suggests that the close agreement of PFC1 to EOF and DDFT in the small density limit probably results from a cancellation of errors due to the smaller D and smaller $\Delta\rho^*$ in the PFC1 model.

In the regime where $\Delta > 1$, the results have been fitted with a linear growth law,

$$x = x_0 + v\tau, \tag{34}$$

where the effect of the initial transient was removed by ignoring data for which $x < 100\sigma$. The resulting v as a function of ρ_i from all the models are shown in Fig. 9. As expected, the front velocity increases as the initial density is increased in all the models. It is also apparent that for any given initial density, the velocity obtained from the EOF is the closest approximation to the DDFT among the present PFC models. If the density axis is rescaled by subtracting the density of

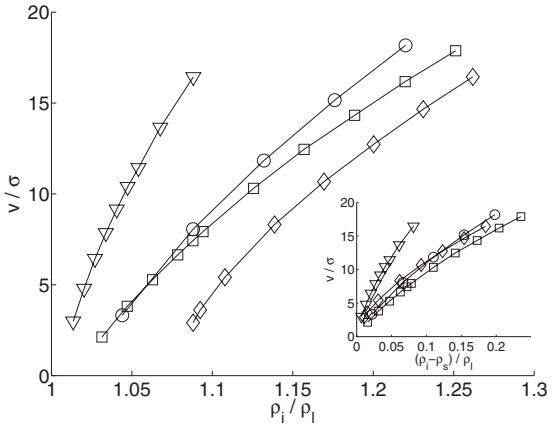

FIG. 9. Growth velocities v obtained in the kinetics controlled regime. Symbols as in Fig. 8.

the solid coexisting with the liquid, the results from FOF seem to agree with DDFT practically as well as those from the EOF, as shown in the inset of Fig. 9. On the other hand, the velocities observed in PFC1 model seem to be a significant overestimation when compared with the results from all the other models studied, even after rescaling the densities. This suggests that the smaller amplitude of density fluctuations and wider crystal-melt surface result in a kinetic barrier which is somewhat smaller than in the other models.

V. CONCLUSIONS

We have presented a new way to derive the eighth-order phase-field crystal model (EOF) from the density functional theory of classical systems. The model was applied to study solidification front dynamics in a two-dimensional ensemble of particles interacting via r^{-12} potential. Predictions from the EOF were compared with similar predictions from dynamical density functional theory (DDFT) of Marconi and Tarazona, and two previously presented phase-field crystal (PFC) models. For the static properties of the system in these models, we find that the DFT predicts freezing of the r^{-12} disks at a density that is about 7% lower than seen in molecular dynamics simulations. From the PFC models studied, we find that the EOF gives the most accurate description of the static properties of the material under study. By studying crystal growth in the diffusion-controlled regime, we find that the EOF gives the best agreement with DDFT among the phase-field crystal models, due to the most accurate description of liquid diffusion constant and solid-liquid coexistence gap in the model. In the regime of interface kinetics controlled growth, we again find the EOF gives closest agreement to the DDFT for all initial densities, although if the initial density is rescaled by the melting point of the solid, the fourth-order fitting scheme slightly outperforms the EOF. These results suggest that among the PFC models studied, the EOF gives the closest approximation to the DDFT. This implies that the EOF is a good candidate for a model to be used for atomistic scale simulations of the growth of two-dimensional hexagonal crystals of Brownian particles, at least in the absence of an external field. In the presence of an external field, a further study would be required to quantify the response in the different models. It should also be noted that while the current study has considered a simple two-dimensional problem, a similar study of the growth of a three dimensional crystal could also quantify the differences in anisotropy of the different phenomena in the models.

ACKNOWLEDGMENTS

We wish to thank Professor K. R. Elder for insightful discussions concerning this work. This work has been supported in part by the Academy of Finland through its Center of Excellence COMP grant and Tekes through its MASIT33 project. A.J. acknowledges support from the Finnish Foundation for Technology Promotion. We also wish to thank CSC-Scientific Computing Ltd. for computational resources.

[1] K. R. Elder, M. Katakowski, M. Haataja, and M. Grant, Phys. Rev. Lett. **88**, 245701 (2002).
[2] K. R. Elder and M. Grant, Phys. Rev. E **70**, 051605 (2004).
[3] H. Emmerich, Adv. Phys. **57**, 1 (2008).
[4] P. Stefanovic, M. Haataja, and N. Provatas, Phys. Rev. Lett. **96**, 225504 (2006).
[5] J. Berry, M. Grant, and K. R. Elder, Phys. Rev. E **73**, 031609 (2006).
[6] G. Tegze, L. Granasy, G. I. Toth, F. Podmaniczky, A. Jaatinen, T. Ala-Nissila, and T. Pusztai, Phys. Rev. Lett. **103**, 035702 (2009).
[7] S. van Teeffelen, R. Backofen, A. Voigt, and H. Löwen, Phys. Rev. E **79**, 051404 (2009).
[8] C. V. Achim, M. Karttunen, K. R. Elder, E. Granato, T. Ala-Nissila, and S. C. Ying, Phys. Rev. E **74**, 021104 (2006).
[9] C. V. Achim, M. Karttunen, K. R. Elder, E. Granato, T. Ala-Nissila, and S. C. Ying, J. Phys.: Conf. Ser. **100**, 072001 (2008).
[10] C. V. Achim, J. A. P. Ramos, M. Karttunen, K. R. Elder, E. Granato, T. Ala-Nissila, and S. C. Ying, Phys. Rev. E **79**, 011606 (2009).
[11] J.-P. Hansen and I. R. McDonald, *Theory of Simple Liquids*, 3rd ed. (Academic, Amsterdam, 2006).
[12] U. M. B. Marconi and P. Tarazona, J. Chem. Phys. **110**, 8032 (1999).
[13] T. V. Ramakrishnan and M. Yussouff, Phys. Rev. B **19**, 2775 (1979).
[14] Y. Singh, Phys. Rep. **207**, 351 (1991).
[15] K. R. Elder, N. Provatas, J. Berry, P. Stefanovic, and M. Grant, Phys. Rev. B **75**, 064107 (2007).
[16] K.-A. Wu and A. Karma, Phys. Rev. B **76**, 184107 (2007).
[17] A. Jaatinen, C. V. Achim, K. R. Elder, and T. Ala-Nissila, Phys. Rev. E **80**, 031602 (2009).
[18] A. Jaatinen, C. V. Achim, K. R. Elder, and T. Ala-Nissila,

Technische Mechanik **30**, 169 (2010).
[19] G. I. Tóth, G. Tegze, T. Pusztai, G. Tóth, and L. Gránásy, J. Phys.: Condens. Matter **22**, 364101 (2010).
[20] H. Lowen, Phys. Rev. E **53**, R29 (1996).
[21] J. Q. Broughton, G. H. Gilmer, and J. D. Weeks, Phys. Rev. B **25**, 4651 (1982).
[22] A. J. Archer and R. Evans, J. Chem. Phys. **121**, 4246 (2004).
[23] J. A. P. Ramos, E. Granato, S. C. Ying, C. V. Achim, K. R. Elder, and T. Ala-Nissila, Phys. Rev. E **81**, 011121 (2010).
[24] S. van Teeffelen, C. N. Likos, and H. Lowen, Phys. Rev. Lett. **100**, 108302 (2008).
[25] A. Jaatinen and T. Ala-Nissila, J. Phys.: Condens. Matter **22**, 205402 (2010).
[26] J. K. Percus and G. J. Yevick, Phys. Rev. **110**, 1 (1958).
[27] J. Berry, K. R. Elder, and M. Grant, Phys. Rev. E **77**, 061506 (2008).
[28] G. Tegze, G. Bansel, G. I. Tóth, T. Pusztai, Z. Fan, and L. Gránásy, J. Comput. Phys. **228**, 1612 (2009); B. P. Vollmayr-Lee, and Andrew D. Rutenberg, Phys. Rev. E **68**, 066703 (2003); J. Zhu, L.-Q. Chen, J. Shen, and V. Tikare, *ibid.* **60**, 3564 (1999).
[29] H. Löwen, J. Bechhoefer, and L. S. Tuckerman, Phys. Rev. A **45**, 2399 (1992).
[30] M. Marder, Phys. Rev. A **45**, R2158 (1992).